

Study of the Radiative Pion Decay

Chuan-Hung Chen¹, Chao-Qiang Geng² and Chong-Chung Lih³

¹*Department of Physics, National Cheng-Kung University, Tainan 701, Taiwan*

²*Department of Physics, National Tsing-Hua University, Hsinchu 300, Taiwan*

³*Department of Optometry, Shu-Zen College of Medicine*

and Management, Kaohsiung Hsien 452, Taiwan

(Dated: August 17, 2018)

Abstract

We study the radiative pion decay of $\pi^+ \rightarrow e^+ \nu_e \gamma$ in the light front quark model (LFQM). We also summarize the result in the chiral perturbation theory. The vector and axial-vector hadronic form factors ($F_{V,A}$) for the $\pi \rightarrow \gamma$ transition are evaluated in the whole allowed momentum transfer. In terms of these momentum dependent form factors, we calculate the decay branching ratio and compare our results with the experimental data and other theoretical predictions in the literature. We also constrain the possible size of the tensor interaction in the LFQM.

I. INTRODUCTION

The light pseudoscalar decays have been playing important roles of understanding the standard model (SM). In particular, the radiative pion decay of $\pi^+ \rightarrow e^+ \nu_e \gamma$ ($\pi_{e2\gamma}$) is an interesting process, which can be used to test the $V - A$ structure of the weak interaction and search for some anomalous interactions beyond the SM. The decay consists of two types of contributions, referred as internal-bremsstrahlung (IB) and structure-dependent (SD) in terms of the emission of the photons, respectively. The IB contribution to the decay amplitude (M_{IB}) is helicity suppressed like the π_{e2} decay as the photon radiates from the external electron, while the SD one (M_{SD}), depending on vector and axial-vector weak hadronic currents, is proportional to the electromagnetic coupling constant α but free of the helicity suppression. One can parametrize M_{SD} by the vector and axial-vector form factors, denote as F_V and F_A , respectively.

The decay of $\pi^+ \rightarrow e^+ \nu_e \gamma$ has been measured with the branching ratio of $(1.61 \pm 0.23) \times 10^{-7}$ for the cuts of $E_\gamma > 21$ MeV and $E_e > 70 - 0.8E_\gamma$ by the ISTRa experiment [1, 2]. Recently, a more precise measurement on the decay branching ratio has been given by the PIBETA Collaboration [3, 4], with the decay branching ratios in various kinematic regions. In particular, for the cuts of $E_e > 0.5$ MeV and $E_\gamma > 10$ MeV with the relative angle $\theta_{e\gamma} > 40^\circ$, the decay branching ratio is $(73.86 \pm 0.54) \times 10^{-8}$ [4]. The new ongoing PEN experiment at PSI will at least double the PIBETA data set [5], resulting in further improvements in precision [6]. In addition, there is another ongoing new experiment, PIENU, at TRIUMF [7] with a similar sensitivity as the PEN experiment.

Theoretical calculations on $F_{V,A}$ as well as the decay branching ratio in the SM have been done in various QCD models [11–17]. In particular, the decay branching ratio with the same cuts as those by ISTRa [1, 2] and PIBETA [4] is found to be 2.55×10^{-7} and 76.66×10^{-8} in the chiral perturbation theory (ChPT) at $O(p^6)$ [8–10], which are larger than the data shown above, respectively. As a result, it may be necessary to consider some new types of interactions, such as tensor interactions [1, 11–15]. It is clear that these tensor interactions are undoubtedly signals of new physics. On the other hand, it is important if we can obtain information on $F_{V,A}$ in some QCD models other than the ChPT. For this purpose, in this study we will evaluate $F_{V,A}$ in the light front quark model (LFQM) [18, 19]. We will use the form factors in both ChPT and LFQM to examine the decay of $\pi^+ \rightarrow e^+ \nu_e \gamma$. In addition,

we will examine the new physics effect due to the tensor interactions.

This paper is organized as follows. In Sec. II, we summarize the form factors in the $\pi \rightarrow \gamma$ transition within the ChPT and LFQM. In Sec. III, we calculate the decay branching ratio of $\pi^+ \rightarrow e^+ \nu_e \gamma$ in these models. We also compare our results with the experimental data and other theoretical predictions in the literature. We give our conclusions in Sec. IV.

II. THE FORM FACTORS

A. Vector and Axial-vector Form Factors

The decay amplitude for $\pi^+ \rightarrow e^+ \nu_e \gamma$ can be written as: [20, 21]

$$\begin{aligned}
M &= M_{IB} + M_{SD}, \\
M_{IB} &= ie \frac{G_F}{\sqrt{2}} V_{ud} f_\pi m_e \epsilon_\mu^* \bar{u}(p_e) (1 - \gamma_5) \left(\frac{p_\pi^\mu}{p_\pi \cdot q} - \frac{2p_e^\mu + \not{q} \gamma^\mu}{2p_e \cdot q} \right) v(p_\nu), \\
M_{SD} &= -i \frac{G_F}{\sqrt{2}} V_{ud} \epsilon_\mu^* \bar{u}(p_e) \gamma_\alpha (1 - \gamma_5) v(p_\nu) \left[e \frac{F_A}{m_\pi} (-g^{\mu\alpha} p_\pi \cdot q + p_\pi^\mu q^\alpha) + ie \frac{F_V}{m_\pi} \epsilon^{\mu\alpha\beta\lambda} q_\beta p_{\pi\lambda} \right], \quad (1)
\end{aligned}$$

where ϵ_α is the photon polarization vector, p_π , p_e , p_ν , and q are the four momenta of π^+ , e^+ , ν and γ , and f_π and $F_{A,V}$ are the π meson decay constant and the axial-vector and vector form factors, defined by

$$\begin{aligned}
\langle 0 | \bar{s} \gamma^\mu \gamma_5 u | \pi^+(p_\pi) \rangle &= i f_\pi p_\pi^\mu, \\
\langle \gamma(q) | \bar{u} \gamma_\mu \gamma_5 d | \pi(p_\pi) \rangle &= e \frac{F_A}{m_\pi} [(p \cdot q) \epsilon_\mu^* - (\epsilon^* \cdot p) q_\mu], \\
\langle \gamma(q) | \bar{u} \gamma_\mu d | \pi(p_\pi) \rangle &= ie \frac{F_V}{m_\pi} \epsilon^{\mu\alpha\beta\nu} \epsilon_\alpha^* q_\beta p_\nu, \quad (2)
\end{aligned}$$

respectively, with $p = p_\pi - q$ being the transfer momentum. Obviously, M_{IB} has a suppression factor of m_e . The physically accessible kinematics region is $0 \leq p^2 \leq p_{\max}^2 = m_\pi^2$ due to the time-like momentum transfers. In the following discussion, we will first summarize the formulas for $F_{V,A}$ in the ChPT [9, 10] and then evaluate these form factors in the LFQM. We note that similar calculations for the $P \rightarrow \gamma$ ($P = K^+, K^0, D, B$) transitions in the LFQM have been performed in Refs. [22–24].

1. Chiral Perturbation Theory

The tree and loop contributions to $F_{V,A}$ in the ChPT at $O(p^6)$ for the $\pi_{e2\gamma}$ decay have been calculated in Refs. [9, 10]. The explicit forms can be summarized as [22]

$$\begin{aligned}
F_V(p^2) = & \frac{m_\pi}{4\sqrt{2}\pi^2 F_\pi} \left\{ 1 - \frac{256}{3}\pi^2 m_K^2 C_7^r + \frac{64}{3}\pi^2 p^2 C_{22}^r \right. \\
& - \frac{1}{8\pi^2 F_\pi^2} \left[m_\pi^2 \ln\left(\frac{m_\pi^2}{\mu^2}\right) + m_K^2 \ln\left(\frac{m_K^2}{\mu^2}\right) \right. \\
& - \int [m_K^2 - x(1-x)p^2] \ln\left(\frac{m_K^2 - x(1-x)p^2}{\mu^2}\right) dx \\
& \left. \left. - \int [m_\pi^2 - x(1-x)p^2] \ln\left(\frac{m_\pi^2 - x(1-x)p^2}{\mu^2}\right) dx \right] \right\}, \tag{3}
\end{aligned}$$

and

$$\begin{aligned}
F_A(p^2) = & \frac{4\sqrt{2}m_\pi}{F_\pi}(L_9^r + L_{10}^r) - \frac{m_\pi}{6F_\pi^3(2\pi)^8}[22.25(m_\pi^2 - p^2) + 193.4] \\
& - \frac{m_\pi}{2\sqrt{2}\pi^2 F_\pi^3} \left\{ (L_3^r + 2L_9^r + 2L_{10}^r) m_K^2 \ln\left(\frac{m_K^2}{m_\rho^2}\right) \right. \\
& \left. + 2(2L_1^r - L_2^r + L_3^r + 2L_9^r + 2L_{10}^r) m_\pi^2 \ln\left(\frac{m_\pi^2}{m_\rho^2}\right) \right\} \\
& - \frac{4\sqrt{2}m_\pi}{F_\pi^3} \left\{ 4m_K^2(6y_{18}^r - 2y_{82}^r + y_{84}^r + 2y_{103}^r) \right. \\
& + 2m_\pi^2(6y_{17}^r + 6y_{18}^r - 2y_{81}^r - 2y_{82}^r + 2y_{83}^r + y_{84}^r + y_{85}^r - y_{100}^r + 2y_{102}^r \\
& \left. + 2y_{103}^r - 2y_{104}^r + y_{109}^r) + \frac{1}{2}(m_\pi^2 - p^2)(2y_{100}^r - 4y_{109}^r + y_{110}^r) \right\}, \tag{4}
\end{aligned}$$

where the wave function and decay constant ($F_\pi \equiv f_\pi/\sqrt{2}$) renormalizations have been included and C_i^r , L_i^r and y_i^r are the renormalized coupling constants. Note that the first terms in Eqs. (3) and (4) correspond to F_V and F_A at $O(p^4)$ [8, 25], respectively. To get the numerical results for the form factors, we take $m_K = 0.495$ GeV, $m_\pi = 0.14$ GeV and $m_\rho = 0.77$ GeV, $F_\pi = 0.092$ GeV and the renormalized coefficients of $(L_1^r, L_2^r, L_3^r, L_9^r, L_{10}^r)$, (C_7^r, C_{22}^r) and $(y_{100}^r, y_{104}^r, y_{109}^r, y_{110}^r)$ to be $(0.53, 0.71, -2.72, 6.9, -5.5) \times 10^{-3}$ [26], $(0.013, 6.52) \times 10^{-3} GeV^{-2}$ [27] and $(1.09, -0.36, 0.40, -0.52) \times 10^{-4}/F_\pi^2$ [28], respectively. For some other possible sets of coefficients, see Ref. [10] as well as the recent review in Ref. [29]. Note that the uncertainties for the renormalized coupling constants are not considered in this study.

2. Light Front Quark Model

In the light front (LF) approach, the general structure of the phenomenological LF meson wave function is based only on the $Q\bar{q}$ Fock space sector [22]. The pion wave function can be expressed by an anti-quark \bar{q} and a quark Q with the total momentum $(p+q)$ as:

$$|\pi(p+q)\rangle = \sum_{\lambda_1\lambda_2} \int [dk_1][dk_2] 2(2\pi)^3 \delta^3(p+q-k_1-k_2) \\ \times \Phi_\pi^{\lambda_1\lambda_2}(z, k_\perp) b_{\bar{q}}^+(k_1, \lambda_1) d_Q^+(k_2, \lambda_2) |0\rangle, \quad (5)$$

where $\Phi_\pi^{\lambda_1\lambda_2}$ is the amplitude of the corresponding $\bar{q}(Q)$ and $k_{1(2)}$ is the on-mass shell LF momentum of the internal quark. The LF relative momentum variables (z, k_\perp) are defined by

$$k_1^+ = (1-z)(p+q)^+, \quad k_2^+ = z(p+q)^+, \\ k_{1\perp} = (1-z)(p+q)_\perp + k_\perp, \quad k_{2\perp} = z(p+q)_\perp - k_\perp, \quad (6)$$

and

$$\Phi_\pi^{\lambda_1\lambda_2}(z, k_\perp) = \left(\frac{k_1^+ k_2^+}{2[M_0^2 - (m_Q - m_{\bar{q}})^2]} \right)^{\frac{1}{2}} \bar{u}(k_1, \lambda_1) \gamma^5 v(k_2, \lambda_2) \phi(z, k_\perp), \\ M_0^2 = \frac{k_\perp^2 + m_q^2}{1-z} + \frac{k_\perp^2 + m_Q^2}{z}. \quad (7)$$

where $\phi(z, k_\perp)$ is the space part of the wave function, which is taken to be a Gaussian type but it can be solved in principle by the LF QCD bound state equation [24]. At the quark loop diagram, the hadronic matrix elements in Eq. (2) can be obtained to be

$$\langle \gamma(q) | \bar{u} \gamma_\mu (1 - \gamma_5) d | \pi(p+q) \rangle = \int \frac{d^4 k_1}{(2\pi)^4} \Lambda_\pi \\ \times \left\{ \gamma_5 \frac{i(-\not{k}'_2 + m_u)}{k_2^2 - m_u^2 + i\epsilon} i e_u \not{\epsilon}^* \frac{i(\not{k}'_3 + m_u)}{k_3^2 - m_u^2 + i\epsilon} \gamma_\mu (1 - \gamma_5) \frac{i(\not{k}'_1 + m_d)}{k_1^2 - m_d^2 + i\epsilon} \right. \\ \left. + (u \leftrightarrow d, k_1 \leftrightarrow k_2) \right\}, \quad (8)$$

where Λ_π is a vertex function related to the quark-antiquark bound state of the π meson, $k_2 = q - k_3$ and $k_1 = (p+q) - k_2 = k_3 + p$. By integrating over the LF momentum k_2^- in Eq. (8), we get

$$\langle \gamma(q) | \bar{u} \gamma_\mu (1 - \gamma_5) d | \pi(p+q) \rangle \\ = \int_p^{p+q} [d^3 k_1] \left\{ \frac{\Lambda_\pi}{k_1^- - k_{1on}^-} (I^\mu |_{k_{2on}^-}) \frac{1}{k_3^- - k_{3on}^-} + (u \leftrightarrow d, k_1 \leftrightarrow k_2) \right\}, \quad (9)$$

where

$$\begin{aligned}
[d^3 k_1] &= \frac{dk_1^+ dk_{1\perp}}{2(2\pi)^3 k_1^+ k_2^+ k_3^+} , \\
I^\mu|_{k_{2on}^-} &= Tr \left\{ \gamma_5 (-\not{k}'_2 + m_u) i e_q \not{q}^* (\not{k}'_3 + m_u) \gamma_\mu (1 - \gamma_5) (\not{k}'_1 + m_d) \right\} , \\
k_{ion}^- &= \frac{m_i^2 + k_{i\perp}^2}{k_i^+} , \quad k_{1(2)}^- = p_{on}^- - k_{2(1)on}^- , \quad k_3^- = q^- - k_{1on}^- ,
\end{aligned} \tag{10}$$

with $\{on\}$ representing the on-shell particles. Note that the vertex function Λ_π in Eqs. (8) and (9) include the normalization factor of the wave function and momentum distribution function, given by [19]:

$$\frac{\Lambda_\pi}{k_1^- - k_{1on}^-} = \frac{\sqrt{k_1^+ k_2^+}}{\sqrt{2} M_0} \phi(z, k_\perp) . \tag{11}$$

Note that in Eq. (11), we have take $m_q = m_Q$, i.e., $m_u = m_d$ for π . To calculate the matrix element in Eq. (9), we choose a frame with the transverse momentum $p_\perp = 0$ so that $p^2 = p^+ p^- \geq 0$ covers the entire range of the momentum transfers. Here, the relevant quark momentum variables are

$$k_3^+ = (1 - z')q^+ , \quad k_2^+ = z'q^+ , \quad k_{3\perp} = (1 - z')q_\perp + k'_\perp , \quad k_{2\perp} = z'q_\perp - k'_\perp . \tag{12}$$

By considering the good component as “ $\mu = +$ ”, the hadronic matrix elements in Eq. (2) can be rewritten as:

$$\begin{aligned}
\langle 0 | \bar{s} \gamma^+ \gamma_5 u | \pi(p+q) \rangle &= i f_\pi (p+q)^+ , \\
\langle \gamma(q) | \bar{u} \gamma^+ \gamma_5 d | \pi(p+q) \rangle &= -e \frac{F_A}{2m_\pi} (\epsilon_\perp^* \cdot q_\perp) p^+ , \\
\langle \gamma(q) | \bar{u} \gamma^+ d | \pi(p+q) \rangle &= -ie \frac{F_V}{2m_\pi} \epsilon^{ij} \epsilon_i^* \epsilon_j p^+ .
\end{aligned} \tag{13}$$

Using Eq. (12), the trace part I^μ in Eq. (10) can be carried out. By comparing the last two equations in Eq. (13) with those in Eq. (9), we derive

$$\begin{aligned}
F_A(p^2) &= 4m_\pi \int \frac{dz' d^2 k_\perp}{2(2\pi)^3} \Phi(z, k_\perp^2) \frac{1}{1-z} \left\{ \frac{1}{3} \frac{m_d + B k_\perp^2 \Theta}{m_d^2 + k_\perp^2} + \frac{2}{3} \frac{m_u - A k_\perp^2 \Theta}{m_u^2 + k_\perp^2} \right\} , \\
F_V(p^2) &= -4m_\pi \int \frac{dz' d^2 k_\perp}{2(2\pi)^3} \Phi(z, k_\perp^2) \frac{1}{1-z} \\
&\quad \times \left\{ \frac{1}{3} \frac{m_d + (1-z)(m_d - m_u) k_\perp^2 \Theta}{m_d^2 + k_\perp^2} - \frac{2}{3} \frac{m_u - z(m_d - m_u) k_\perp^2 \Theta}{m_u^2 + k_\perp^2} \right\} ,
\end{aligned} \tag{14}$$

where

$$\begin{aligned}
A &= z(1 - 2z')(m_d - m_u) - 2z'm_u, \\
B &= z(1 - 2z')m_d + m_d + (1 - 2z')(1 - z)m_u, \\
\Phi(z, k_\perp^2) &= 4 \left(\frac{\pi}{\omega_\pi^2} \right)^{\frac{3}{4}} \left(\frac{z(1 - z)}{2[M_0^2 - (m_d - m_u)^2]} \right)^{1/2} \sqrt{\frac{dk_z}{dz}} \exp \left(-\frac{\vec{k}^2}{2\omega_\pi^2} \right), \\
\Theta &= \frac{1}{\Phi(z, k_\perp^2)} \frac{d\Phi(z, k_\perp^2)}{dk_\perp^2}, \\
z &= z' \left(1 - \frac{p^2}{m_\pi^2} \right), \quad \vec{k} = (\vec{k}_\perp, \vec{k}_z), \\
k_z &= \left(z - \frac{1}{2} \right) M_0 + \frac{m_d^2 - m_u^2}{2M_0}.
\end{aligned} \tag{15}$$

We note that to evaluate the form factors, we have to fix the meson scale parameter ω_π in the meson wave functions by fitting the meson decay constant, given by [30]

$$f_\pi = \sqrt{48} \int \frac{dz d^2k_\perp}{2(2\pi)^3} \Phi(z, k_\perp) \frac{m_u}{z(1 - z)}. \tag{16}$$

B. Tensor Form Factor

The tensor interaction is given by [11, 14]

$$\mathcal{L}_T = \frac{G_F}{\sqrt{2}} \sin \theta_c f_T (\bar{u} \sigma_{\mu\nu} \gamma_5 d) [\bar{e} \sigma^{\mu\nu} (1 - \gamma_5) \nu_e]. \tag{17}$$

The tensor form factor is defined by [14]:

$$\langle \gamma(q) | \bar{u} \sigma_{\mu\nu} \gamma_5 d | \pi(p_\pi) \rangle = -i \frac{eF_T}{2f_T} (\epsilon_\mu^* q_\nu - q_\mu \epsilon_\nu^*). \tag{18}$$

For the LF good component of “ $\mu = +$ ”, one rewrites Eq. (18) as

$$\langle \gamma(q) | \bar{u} \sigma^{+\nu} \gamma_5 d | \pi(p + q) \rangle = -i \frac{eF_T}{2f_T} (\epsilon_\perp^* \cdot q_\perp). \tag{19}$$

At the quark level, the hadronic matrix element in Eq. (18) is found to be

$$\begin{aligned}
&\langle \gamma(q) | \bar{u} \sigma_{\mu\nu} \gamma_5 d | \pi(p + q) \rangle = \\
&\int \frac{d^4k'_1}{(2\pi)^4} \Lambda_\pi \left\{ \gamma_5 \frac{i(-k'_2 + m_u)}{k_2^2 - m_u^2 + i\epsilon} i e_u \not{\epsilon}^* \frac{i(k'_3 + m_u)}{k_3^2 - m_u^2 + i\epsilon} \sigma_{\mu\nu} \gamma_5 \frac{i(k'_1 + m_d)}{k_1^2 - m_d^2 + i\epsilon} + (u \leftrightarrow d, k_1 \leftrightarrow k_2) \right\},
\end{aligned} \tag{20}$$

which leads to

$$\begin{aligned}
&\langle \gamma(q) | \bar{u} \sigma_\mu \gamma_5 d | \pi(p + q) \rangle = \\
&\int_p^{p+q} [d^3k_1] \left\{ \frac{\Lambda_\pi}{k_1^- - k_{1on}^-} (I^{\mu\nu} |_{k_{2on}^-}) \frac{1}{k_3^- - k_{3on}^-} + (u \leftrightarrow d, k_1 \leftrightarrow k_2) \right\},
\end{aligned} \tag{21}$$

where

$$I^{\mu\nu}|_{k_{2on}^-} = Tr \left\{ \gamma_5 (-\not{k}'_2 + m_u) i e_q \not{q}^* (\not{k}'_3 + m_u) \sigma_\mu \gamma_5 (\not{k}'_1 + m_d) \right\}. \quad (22)$$

From Eqs. (19) and (21), we obtain

$$\frac{F_T(p^2)}{f_T} = 2 \int \frac{dz' d^2 k_\perp}{2 (2\pi)^3} \Phi(z, k_\perp^2) \left\{ \frac{2 C_1 + C_2 k_\perp^2 \Theta}{3 m_u^2 + k_\perp^2} + \frac{1}{3} (m_d \leftrightarrow m_u) \right\}, \quad (23)$$

where

$$\begin{aligned} C_1 &= \frac{1}{z' z (1-z)^2 (1-z')} \left\{ (1-2z' + 2z'^2 - z'z)(z' + z - 2z'z) k_\perp^2 \right. \\ &\quad \left. + (1-z) m_u [2z'z(1-z') m_d + (z' + z + 2z'^2 z - 4z'z) m_d] \right\}, \\ C_2 &= \frac{(z-z')}{z' z (1-z)^2 (1-z')} \left\{ (z' + z - 2z'z) k_\perp^2 + z^2 (1-z') m_d^2 \right. \\ &\quad \left. - (1-z)(z' + z - z'z) m_u^2 \right\}. \end{aligned} \quad (24)$$

At the maximal recoil of $p^2 = 0$, we have

$$\begin{aligned} \frac{F_T(0)}{f_T} &= 4 \int \frac{dz d^2 k_\perp}{2 (2\pi)^3} \Phi(z, k_\perp^2) \left\{ \frac{2(1-z)k^2 + m_u(z m_d + (1-z)m_u)}{z(m_u^2 + k_\perp^2)} \right. \\ &\quad \left. + \frac{1}{3} (m_u \leftrightarrow m_d) \right\}. \end{aligned} \quad (25)$$

C. Numerical results

To compute numerical values of the form factors in the LFQM, the ω parameter in the light-front wave function is fixed by other hadronic properties. For example, by using the decay constant of $f_\pi = 130$ MeV and the quark masses of $m_u = m_d = 250$ MeV, we obtain $\omega_\pi = 301$ MeV from Eq. (16). We note that this value of ω_π is just a typical one and its uncertainty mainly arises from those of the light quark masses. The transfer momentum p^2 dependences of F_V and F_A are shown in Figs. 1 and 2, respectively. Note that the behaviors of the figure's sharps are independent of the quark masses but the values of F_V and F_A at the maximal recoil of $p^2 = 0$ can be quite different as shown in Table I. The results in Table I also illustrate the main uncertainty from the quark masses. In Figs. 1 and 2, we have also included the experimental results fitted by the forms of $F_V(p^2) = F_V(1 + \alpha p^2)$

and $F_A(p^2) = F_A(0)$ with a constant parameter of α [4], while in Table. I, we list the values of $F_{A,V}(0)$ in the ChPT and those from the data. We remark that the numerical values of the form factors at $p^2 = 0$ for the pion case between the theoretical models seem to be less compatible comparing with those for the kaon in Ref. [10] in which the strange quark mass also enters. To illustrate the quark mass effects on the form factors in the LFQM, in Figs. 3 and 4 we plot three different sets of quark masses including the one in Figs. 1 and 2. It is clear that both $F_{V,A}$ decrease as $m_{u,d}$ increase.

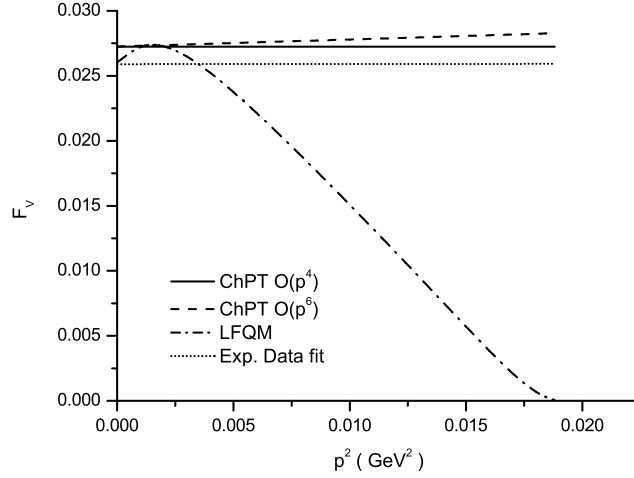


FIG. 1. $F_V(p^2)$ as a function of the transfer momentum p^2 with $m_u = m_d = 250$ MeV.

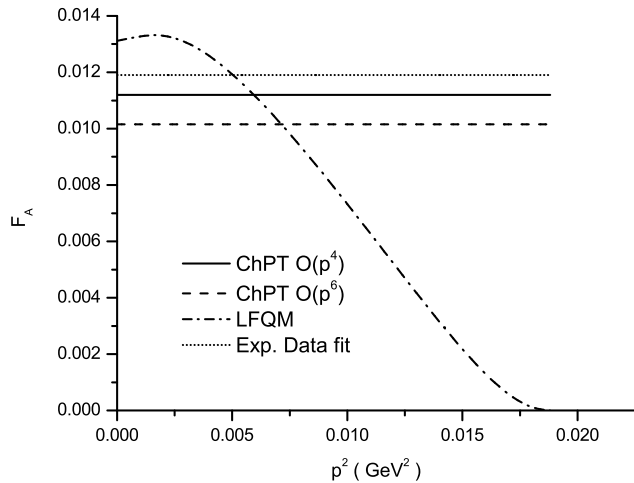


FIG. 2. Same as Fig. 1 but for $F_V(p^2)$.

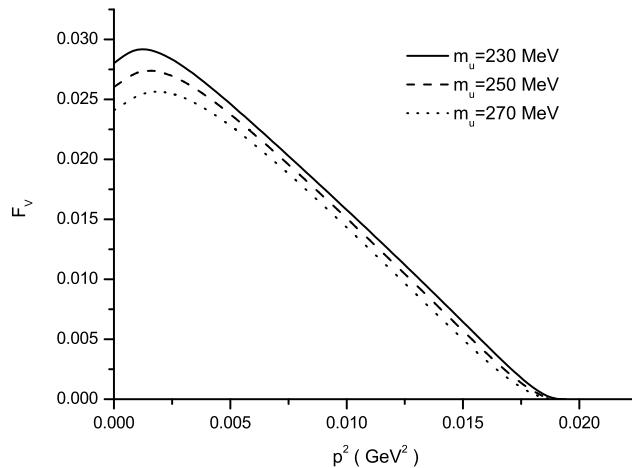


FIG. 3. $F_V(p^2)$ in the LFQM, where $m_u = m_d = 230, 250$ and 270 MeV correspond to solid, long-dashed and short-dashed lines, respectively.

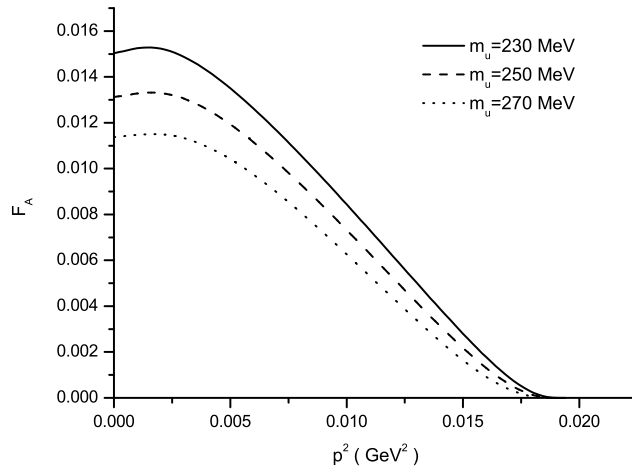


FIG. 4. Same as Fig. 3 but for $F_V(p^2)$.

TABLE I. Values of $F_{A,V}(0)$ in (a) the ChPT at $O(p^4)$, (b) the ChPT at $O(p^6)$, (c) the LFQM with $i=1, 2$ and 3 for $m_{u,d} = 230, 250$ and 270 MeV, respectively.

	(a)	(b)	(c1)	(c2)	(c3)	Data [4]
$F_A(0)$	0.0112	0.0102	0.0151	0.0131	0.0113	0.0117(17)
$F_V(0)$	0.0272	0.0272	0.02751	0.0261	0.0243	0.0258(17)

The tensor form factor Eq. (23) in the whole kinematic region for the LFQM is shown in Fig. 5. At $p^2 = 0$, we get the $F_T(0)/f_T = 0.220$, 0.210 and 0.202 for $m_{u,d} = 230$, 250 and 270 MeV, respectively.

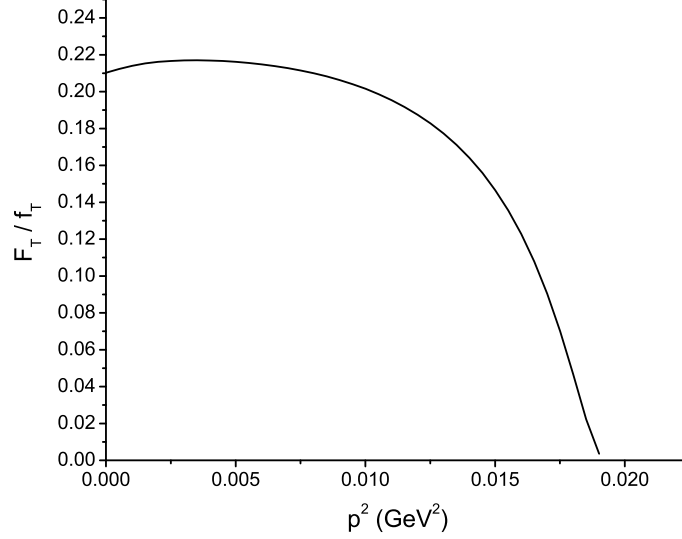


FIG. 5. $\frac{F_T(p^2)}{f_T}$ as a function of the transfer momentum p^2 .

270 MeV, respectively.

III. DECAY BRANCHING RATIO

In the π^+ rest frame, we obtain the double differential decay rate as

$$\frac{d^2\Gamma^l}{dx dy} = \frac{m_\pi}{256\pi^3} |M|^2 = \frac{\alpha}{2\pi} Br(\pi \rightarrow e\nu) A, \quad (26)$$

$$A = A_{IB}(x, y) + A_{SD}(x, y) + A_{INT}(x, y), \quad (27)$$

with

$$\begin{aligned} A_{IB}(x, y) &= \frac{1-\lambda}{\lambda x^2} \left[x^2 + 2(1-r_e) \left(1 - x - \frac{r_e}{\lambda} \right) \right], \\ A_{SD}(x, y) &= \frac{m_\pi^4(1-\lambda)}{4f_\pi^2 m_e^2} x^2 \left[|F_V + F_A|^2 \frac{\lambda^2}{1-\lambda} \left(1 - x - \frac{r_e}{\lambda} \right) \right. \\ &\quad \left. + |F_V - F_A|^2 (y - \lambda) \right], \\ A_{IN}(x, y) &= -\frac{m_\pi}{f_\pi} \left[Re[(F_V + F_A)^*] \left(1 - x - \frac{r_e}{\lambda} \right) \right. \\ &\quad \left. - Re[(F_V - F_A)^*] \frac{1-y+\lambda}{\lambda} \right], \end{aligned} \quad (28)$$

where $x = 2E_\gamma/m_\pi$, $y = 2E_e/m_\pi$, $r_e = m_e^2/m_\pi^2$ and $\lambda = (x + y - 1 - r_e)/x$. One can also relate the angle $\theta_{e\gamma}$ between the e^+ and photon momenta with y and λ . Explicitly, by neglecting the r_e , one has that

$$\lambda = y \sin^2 \left(\frac{\theta_{e\gamma}}{2} \right). \quad (29)$$

The physical regions for x and y are given by

$$\begin{aligned} 0 &\leq x \leq 1 - r_e, \\ 1 - x + \frac{r_e}{1-x} &\leq y \leq 1 + r_e. \end{aligned} \quad (30)$$

In Table II, we show the decay branching fractions of $\pi^\pm \rightarrow e^\pm \nu_e \gamma$ in terms of the various contributions in Eq. (28) for $f_\pi = 130$ MeV, $m_\pi = 140$ GeV [2], $m_{u,d} = 250$ MeV and $Br(\pi \rightarrow e\nu) = (1.23 \pm 0.004) \times 10^{-8}$ with the cuts of $E_\gamma > 50$ MeV and $E_e > 50$ MeV. Note that in this kinematic region, the contribution from the SD part dominates the decay rate, which is sensitive to the $V - A$ structure as well as new physics. We note that the total branching ratio in the LFQM are 2.937 and 2.320×10^{-8} for $m_{u,d} = 230$ and 270 MeV, respectively.

TABLE II. Decay branching ratio of $\pi \rightarrow e\nu_e\gamma$ (in units of 10^{-8}) in (a) the ChPT at $O(p^4)$, (b) the ChPT at $O(p^6)$ and (c) the LFQM with the cuts of $E_\gamma > 50$ MeV and $E_e > 50$ MeV, respectively.

Model	IB	SD	INT	Total
(a)	3.692×10^{-1}	2.356	2.536×10^{-3}	2.727
(b)	3.692×10^{-1}	2.309	2.850×10^{-3}	2.679
(c)	3.692×10^{-1}	2.250	1.840×10^{-3}	2.621

In Table III, we give the decay branching ratio of $\pi \rightarrow e\nu_e\gamma$ in various kinematic energy regions in (a) the ChPT at $O(p^4)$, (b) the ChPT at $O(p^6)$, (c) the LFQM, (d) the green function method [16] and (e) the ChPT with a large N_C expansion [17] as well as the data in Ref. [4]. Here, we have used $m_{u,d} = 250$ MeV in the LFQM. The errors in the parentheses of our results in Table III are from the decay of $\pi \rightarrow e\nu$. However, it should be noted that large uncertainties could arise from the various normalized coupling constants and the light quark masses in the ChPT and LFQM, respectively. In Fig. 6, we display the spectrum of the differential decay branching ratio as a function of $x = 2E_\gamma/m_\pi$ in the ChPT at both

TABLE III. Decay branching ratio of $\pi \rightarrow e\nu_e\gamma$ (in units of 10^{-8}) in (a) the ChPT at $O(p^4)$, (b) the ChPT at $O(p^6)$, (c) the LFQM with $i=1, 2$ and 3 for $m_{u,d} = 230, 250$ and 270 MeV, respectively, (d) the green function method [16] and (e) the ChPT with a large N_C expansion [17] as well as the data in Ref. [4] in various kinematic energy regions (in units of MeV).

E_e^{min}	E_γ^{min}	$\theta_{e\gamma}^{min}$	Data [4]	(a)	(b)	(c1)	(c2)	(c3)	(d)	(e)
50	50	—	2.614(21)	2.727(9)	2.679(9)	2.85(8)	2.62(8)	2.29(8)	2.81(38)	2.58(8)
10	50	40^0	14.46(22)	15.04(5)	14.99(5)	14.93(37)	14.63(37)	14.19(37)	15.08(58)	14.77(40)
50	10	40^0	37.69(46)	38.28(13)	38.12(12)	38.29(12)	37.87(12)	37.37(12)	38.4(10)	38.9(9)
0.5	10	40^0	73.86(54)	76.66(25)	76.31(25)	73.67(22)	73.57(22)	72.58(22)	—	—

$O(p^4)$ and $O(p^6)$ and the LFQM. From Table III, we see that the results of the ChPT at

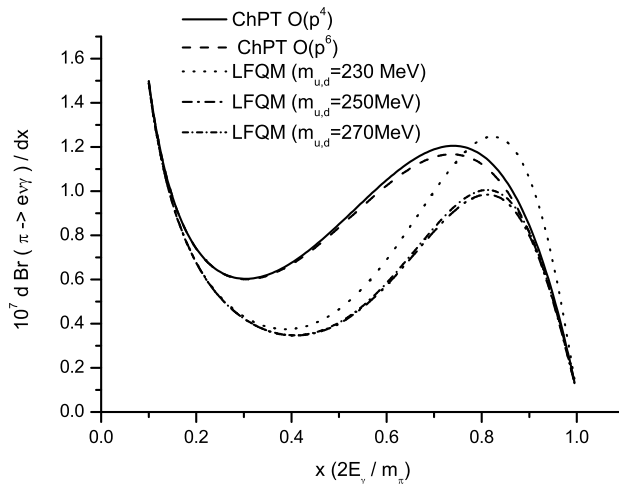


FIG. 6. Differential decay branching ratio as a function of $x = 2E_\gamma/m_\pi$.

$O(p^4)$ and $O(p^6)$ are higher than those of the experimental data, which can be understood from Table I and Eq. (28) since the values of $F_{V-A}(0) \equiv F_V(0) - F_A(0)$ in the ChPT are larger than those fitted in the experimental data. Since the result from the LFQM agrees well with the data [4], it could lead to a strong constraint on new physics. We now examine the contribution to the decay from the tensor interaction in Eq. (17). From Eqs. (17) and (18), one obtains the new tensor contribution as

$$M_T = ie \frac{G_F}{\sqrt{2}} \sin \theta_c (F_T \epsilon_\mu^* q_\nu) [\bar{l} \sigma^{\mu\nu} (1 - \gamma_5) \nu_l]. \quad (31)$$

Due to the above tensor interaction, Eq. (27) should be rewritten as follows:

$$A = A_{IB}(x, y) + A_{SD}(x, y) + A_{INT}(x, y) + A_{TT}(x, y) + A_{IBT}(x, y) + A_{SDT}(x, y), \quad (32)$$

where the new terms are given by

$$\begin{aligned} A_{TT}(x, y) &= \frac{m_\pi^4}{f_\pi^2 m_e^2} |F_T|^2 x^2 \lambda(1 - \lambda), \\ A_{IBT}(x, y) &= 2 \frac{m_\pi^2}{f_\pi m_e} \text{Re}(F_T) \left(1 + r_e - \lambda - \frac{r_e}{\lambda}\right), \\ A_{SDT}(x, y) &= \frac{m_\pi^3}{f_\pi^2 m_e} \text{Re}(F_T) (F_V - F_A) x^2 \lambda(1 - \lambda). \end{aligned} \quad (33)$$

Integrating over x and y variables in Eq.(33) and using the form factor in Eq.(23), we get the tensor related parts of the branching ratio as shown in Table. IV. To evaluate the

TABLE IV. The tensor related parts of the decay branching ratio for $\pi \rightarrow e\nu_e\gamma$ (in units of 10^{-8}) in the LFQM with the cuts of $E_\gamma > 50$ MeV and $E_e > 50$ MeV.

TT	SDT	IBT
$4.636 \times 10^2 f_T^2$	$9.817 \times 10^{-2} f_T$	$2.536 \times 10 f_T$

total branching ratio including the tensor part, we can combine the results in Tables II and IV. By comparing the final result with the experimental data of $\pi^\pm \rightarrow e^\pm \nu_e \gamma$, we extract $f_T = (3.48_{-8.23}^{+8.02}) \times 10^{-4}$ shown in Table V in the LFQM for $m_{u,d} = 250$ MeV. In the table, we

TABLE V. Form factor of f_T in units of 10^{-4} .

LFQM	[4]	[11]	[13]	[15]	[16]
$3.48_{-8.23}^{+8.02}$	-0.6 ± 2.8	-56 ± 17	372 ± 120	-115 ± 33	1 ± 14

have also given other results in the literature including the single tensor form factor fitted by PIBETA [4]. We note that our result in the LFQM and that by PIBETA correspond to $-1.0 \times 10^{-3} < f_T < 1.66 \times 10^{-3}$ and $-5.2 \times 10^{-4} < f_T < 4.0 \times 10^{-4}$ at 90% C.L., respectively.

IV. CONCLUSIONS

We have studied the momentum dependent $\pi \rightarrow \gamma$ transition form factors $F_{A,V}(p^2)$ in the ChPT and LFQM. In particular, we have found that $F_A(0) = 0.0112, 0.0102$, and

(0.151, 0.0131, 0.0113) and $F_V(0) = 0.0272, 0.0272,$ and (0.0275, 0.0261, 0.0243) in (a) the ChPT $O(p^4)$, (b) the ChPT $O(p^6)$, and (c) the LFQM with $m_{u,d} = (230, 250, 270)$ MeV, respectively, at the maximal recoil of $p^2 = 0$. Based on these form factors, we have calculated the decay branching ratio of $\pi \rightarrow e\nu_e\gamma$. Explicitly, we have obtained that in the SM with the cut of $E_\gamma > m_e$ and $E_e > 10$ MeV with the relative angle $\theta_{e\gamma} > 40^\circ$, the decay branching ratio is $76.66 \pm 0.25, 76.31 \pm 0.25$ and $(73.67 \pm 0.22, 73.57 \pm 0.22, 72.58 \pm 0.22) \times 10^{-8}$ in (a), (b) and (c), respectively, while the experimental measurement is 73.86×10^{-8} by the PIBETA Collaboration. Since our results fit well with the data, we have also derived a constraint for the tensor interaction to be $-1.0 \times 10^{-3} < f_T < 1.66 \times 10^{-3}$ at 90% C.L. in the LFQM .

V. ACKNOWLEDGMENTS

We thank Professors D.A. Bryman and T. Numa0 for useful discussions. This work is supported in part by the National Science Council of R.O.C. under Grant #s: NSC97-2112-M-006-001-MY3 (CHC), NSC-95-2112-M-007-059-MY3 (CQG), NSC-98-2112-M-007-008-MY3 (CQG) and NSC-97-2112-M-471-002-MY3 (CCL) and by the Boost Program of NTHU (CQG).

-
- [1] V. N. Bolotov *et. al.*, Phys. Lett. **B243** (1990) 308; Sov. J. Nucl. Phys. **51** (1990) 455.
 - [2] C. Amsler *et al.* [Particle Data Group], Phys. Lett. B **667** (2008) 1.
 - [3] E. Frlez, *et. al.*, Phys. Rev. Lett **93** (2004) 181804.
 - [4] M. Bychkov *et al.*, Phys. Rev. Lett. **103** (2009) 051802.
 - [5] See the PENCollaboration Home Page at <http://pen.phys.virginia.edu/> and references therein.
 - [6] D. Pocanic *et al.* [PEN Collaboration], arXiv:0909.4360 [hep-ex]; see also D. Pocanic, arXiv:1004.4192 [hep-ex].
 - [7] D. Bryman, PoS **KAON** (2008) 052.
 - [8] J. Bijnens, G. Ecker and J. Gasser, Nucl. Phys. **B396** (1993) 81.
 - [9] L. Ametller, J. Bijnens, A. Braman and F. Cornet, Phys. Lett. **B303** (1993) 140.
 - [10] C. Q. Geng, I. L. Ho and T. H. Wu, Nucl. Phys. **B684** (2004) 281.

- [11] A. A. Poblaguev, Phys. Lett. B **238** (1990) 108.
- [12] V. M. Belyaev and I. I. Kogan, Phys. Lett. B **280**, 238 (1992); Yu. Y. Komachenko, Sov. J. Nucl. Phys. **55**, 1384 (1992) [Yad. Fiz. **55**, 2487 (1992)].
- [13] M. V. Chizhov, Mod. Phys. Lett. **A8** (1993) 2753; Phys. Part. Nucl. Lett. **2** (2005) 193.
- [14] C. Q. Geng and S. K. Lee, Phys. Rev. **D51** (1995) 99.
- [15] A. A. Poblaguev, Phys. Rev. **D68** (2003) 054020.
- [16] V. Mateu and J. Portoles, Eur. Phys. J. C **52**, 325 (2007) [arXiv:0706.1039 [hep-ph]].
- [17] R. Unterdorfer and H. Pichl, Eur. Phys. J. C **55**, 273 (2008) [arXiv:0801.2482 [hep-ph]].
- [18] W. M. Zhang and A. Harindranath, Phys. Rev. **D48**, 4881 (1993); K. G. Wilson *et al.*, Phys.Rev. **D49**, 6720 (1994); W. M. Zhang, Phys. Rev. **D56** (1997) 1528.
- [19] W. Jaus, Phys. Rev. **D41**, 3394 (1990); **44**, 2851 (1991); Demchuk et al., Phys. Atom. Nucl **59**, 2152 (1996).
- [20] D. A. Bryman *et al.*, Phys. Rep. **88**, 151 (1982).
- [21] C. H. Chen, C. Q. Geng and C. C. Lih, Phys. Rev. D **56**, 6856 (1997).
- [22] C. H. Chen, C. Q. Geng and C. C. Lih, Phys. Rev. D **77**, 014004 (2008); Int. J. Mod. Phys. **A23**, 3204 (2008).
- [23] C. Q. Geng, C. C. Lih and C. C. Liu, Phys. Rev. **D62** (2000) 034019.
- [24] C. Q. Geng, C. C. Lih and W. M. Zhang, Phys. Rev. D **57**, 5697 (1998); Phys. Rev. D **62**, 074017 (2000); Mod. Phys. Lett. A **15**, 2087 (2000); C. C. Lih, C. Q. Geng and W. M. Zhang, Phys. Rev. D **59**, 114002 (1999).
- [25] J. F. Donoghue and B. R. Holstein, Phys. Rev. **D40**, 2378 (1989); Phys. Rev. **D40**, 3700 (1989).
- [26] G. Amoros, J. Bijnens and P. Talavera, Nucl. Phys. B **602**, 87 (2001)
- [27] O. Strandberg, arXiv:hep-ph/0302064.
- [28] M. Knecht and A. Nyffeler, Eur. Phys. J. C **21**, 659 (2001).
- [29] J. Bijnens, Prog. Part. Nucl. Phys. **58**, 521 (2007), and references therein.
- [30] C. Q. Geng, C. W. Hwang, C. C. Lih and W. M. Zhang, Phys. Rev. D **64**, 114024 (2001); C. H. Chen, C. Q. Geng, C. C. Lih and C. C. Liu, Phys. Rev. D **75**, 074010 (2007).